NASA/TM—2007-214802

Failure Maps for Rectangular 17-4PH Stainless Steel Sandwiched Foam Panels

S.V. Raj
Glenn Research Center, Cleveland, Ohio

L.J. Ghosn
Ohio Aerospace Institute, Brook Park, Ohio

May 2007

NASA STI Program . . . in Profile

Since its founding, NASA has been dedicated to the advancement of aeronautics and space science. The NASA Scientific and Technical Information (STI) program plays a key part in helping NASA maintain this important role.

The NASA STI Program operates under the auspices of the Agency Chief Information Officer. It collects, organizes, provides for archiving, and disseminates NASA's STI. The NASA STI program provides access to the NASA Aeronautics and Space Database and its public interface, the NASA Technical Reports Server, thus providing one of the largest collections of aeronautical and space science STI in the world. Results are published in both non-NASA channels and by NASA in the NASA STI Report Series, which includes the following report types:

- TECHNICAL PUBLICATION. Reports of completed research or a major significant phase of research that present the results of NASA programs and include extensive data or theoretical analysis. Includes compilations of significant scientific and technical data and information deemed to be of continuing reference value. NASA counterpart of peer-reviewed formal professional papers but has less stringent limitations on manuscript length and extent of graphic presentations.

- TECHNICAL MEMORANDUM. Scientific and technical findings that are preliminary or of specialized interest, e.g., quick release reports, working papers, and bibliographies that contain minimal annotation. Does not contain extensive analysis.

- CONTRACTOR REPORT. Scientific and technical findings by NASA-sponsored contractors and grantees.

- CONFERENCE PUBLICATION. Collected papers from scientific and technical conferences, symposia, seminars, or other meetings sponsored or cosponsored by NASA.

- SPECIAL PUBLICATION. Scientific, technical, or historical information from NASA programs, projects, and missions, often concerned with subjects having substantial public interest.

- TECHNICAL TRANSLATION. English-language translations of foreign scientific and technical material pertinent to NASA's mission.

Specialized services also include creating custom thesauri, building customized databases, organizing and publishing research results.

For more information about the NASA STI program, see the following:

- Access the NASA STI program home page at *http://www.sti.nasa.gov*

- E-mail your question via the Internet to *help@sti.nasa.gov*

- Fax your question to the NASA STI Help Desk at 301–621–0134

- Telephone the NASA STI Help Desk at 301–621–0390

- Write to:
  NASA Center for AeroSpace Information (CASI)
  7115 Standard Drive
  Hanover, MD 21076–1320

NASA/TM—2007-214802

Failure Maps for Rectangular 17-4PH Stainless Steel Sandwiched Foam Panels

S.V. Raj
Glenn Research Center, Cleveland, Ohio

L.J. Ghosn
Ohio Aerospace Institute, Brook Park, Ohio

National Aeronautics and
Space Administration

Glenn Research Center
Cleveland, Ohio 44135

May 2007

Acknowledgments

The authors thank Dr. Brian Fite for providing details of the NASA fan blade design and for his advice during the course of this work. This study was funded in part by the ULTRASAFE Project and in part by the Low Emission Alternative Program (LEAP) at the NASA Glenn Research Center.

This work was sponsored by the Fundamental Aeronautics Program at the NASA Glenn Research Center.

Level of Review: This material has been technically reviewed by technical management.

Available from

NASA Center for Aerospace Information
7115 Standard Drive
Hanover, MD 21076–1320

National Technical Information Service
5285 Port Royal Road
Springfield, VA 22161

Available electronically at http://gltrs.grc.nasa.gov

Failure Maps for Rectangular 17-4PH Stainless Steel Sandwiched Foam Panels

S.V. Raj
National Aeronautics and Space Administration
Glenn Research Center
Cleveland, Ohio 44135

L.J. Ghosn
Ohio Aerospace Institute
Brook Park, Ohio 44142

Abstract

A new and innovative concept is proposed for designing lightweight fan blades for aircraft engines using commercially available 17-4PH precipitation hardened stainless steel. Rotating fan blades in aircraft engines experience a complex loading state consisting of combinations of centrifugal, distributed pressure and torsional loads. Theoretical failure plastic collapse maps, showing plots of the foam relative density versus face sheet thickness, t, normalized by the fan blade span length, L, have been generated for rectangular 17-4PH sandwiched foam panels under these three loading modes assuming three failure plastic collapse modes. These maps show that the 17-4PH sandwiched foam panels can fail by either the yielding of the face sheets, yielding of the foam core or wrinkling of the face sheets depending on foam relative density, the magnitude of t/L and the loading mode. The design envelop of a generic fan blade is superimposed on the maps to provide valuable insights on the probable failure modes in a sandwiched foam fan blade.

List of Symbols

a_T	Acceleration of the rotating sandwiched foam panel
A_c	Cross-sectional area of the foam core
A_s	Cross-sectional area of the face sheets
b	Width of a sandwiched foam cantilever panel
B_1	Constant equal to 2 for a sandwiched foam cantilever panel
B_2	Constant equal to about 2
C_1	Constant equal to about unity
E_c	Young's modulus of the foam core
E_{cs}	Young's modulus of the solid unfoamed core
E_s	Young's modulus of the solid material
E_{eff}	Effective Young's modulus of the sandwiched core
G	Shear modulus
G_c	Shear modulus of the foam core
G_{critical}	Critical fracture toughness of brazed interface at which debonding occurs
G_s	Shear modulus of the solid material
I_{pc}	Polar moment of inertia for the foam core under torsional loading
I_{ps}	Polar moment of inertia for the face sheets under torsional loading
L	Length of the sandwiched foam panel

m_T	Total mass of the sandwiched foam panel
P	Axial, bend or impact load
P_c	Axial load acting on the foam core
P_{ind}	Localized indentation load due to foreign object damage (FOD)
P_s	Axial load acting on the face sheets
q	Distributed pressure load acting on a sandwiched foam cantilever panel
r	Radial distance across the cross-section of a sandwiched foam panel
t	Face sheet thickness
t_c	Thickness of the foam core
t_P	Thickness of the sandwiched foam plate = $(2t + t_c)$
T	Total torque on the sandwiched foam panel
T_c	Torque on the foam core
T_s	Torque on the face sheet
γ	Shear strain
ε_c	Elastic strain of the foam core
ε_s	Elastic stain of the face sheets
ε_T	Total strain
ρ_c	Density of the foam core
ρ_{eff}	Effective density of the sandwiched foam structure
ρ_s	Density of solid material
σ_{yc}	Yield strength of the foam core
σ_{ys}	Yield strength of the solid metal
σ_c	Axial stress acting on the foam core
σ_s	Axial stress acting on the face sheets
$(\tau_c)_{\max}$	Maximum shear stress acting on the foam core
$\tau_{\max}$	Maximum shear strength of a sandwiched foam shear specimen
$(\tau_s)_{\max}$	Maximum shear stress acting on the face sheets
υ_c	Poisson's ratio of the foam core
υ_s	Poisson's ratio of the solid material
ϕ	Twist angle
ω	Angular velocity of the rotating sandwiched foam panel

1. Introduction

Recent advances in cellular theory [1-20] and manufacturing techniques [21,22] have created an interest in developing new applications for foam materials in the fabrication of lightweight engineering components [23]. Specifically, metallic foams provide several advantages to the designer due to their diverse multifunctional characteristics and ductility [21,24,25]. For example, metallic foams possess low density, energy absorption and vibration dampening properties along with the ability to be fabricated with curvatures as three-dimensional structures.

The fact that the densities of foams are extremely low compared to that of the solid material is especially advantageous in conceiving new innovative concepts for many common applications. For example, metallic

foams made of relatively inexpensive and common alloys, such as high strength and high toughness aerospace grade 17-4PH stainless steel, can be used in fabricating aircraft engine fan blades to replace more expensive titanium alloys and polymeric composite materials. The proposed blade architecture is a lightweight sandwich construction made up of thin contoured solid face sheets either brazed or solid-state diffusion bonded to a space-filling metallic foam core (fig. 1) [26]. The embedding of a lightweight stainless steel foam core between the two face sheets considerably increases the stiffness of the sandwich blade as compared to simply brazing two sheets. Figure 2 shows a schematic of a NASA[1]-designed blade used in the modeling studies [26]. Detailed analytical studies using this fan blade design have demonstrated that 17-4PH stainless steel fan blades are superior to solid Ti-6(wt.%)Al-4% V fan blades, and possibly even hollow titanium alloy blades, both in terms of rigidity, weight and vibration analyses, simulated impact loading due to a bird strike, and cost [26]. The mechanical properties of 17-4PH sandwiched foam specimens are reported elsewhere [26,27].

Gibson and Ashby (GA) [2] proposed constructing failure[2] plastic collapse maps for specimens consisting of a rigid polyurethane foam core sandwiched between two Al face sheets subjected to bending loads. Since no such maps exist for 17-4PH sandwiched foam panels, the objectives of this paper are to construct similar failure maps. The present paper extends the earlier work by Gibson and Ashby [2] to centrifugal and torsional loading modes for cantilevered 17-4PH sandwiched foam panels. The construction of these maps can provide useful insights into probable failure modes for a 17-4PH sandwich foam fan blade for different combinations of relative densities and fan blade geometries under different loading conditions. A fundamental assumption made in this paper is that the face plates are brazed under proper conditions to the metallic foam core so that failure by debonding at the brazed interfaces is ignored. It is noted that this mode of failure is very likely when the brazed interfaces are weak.

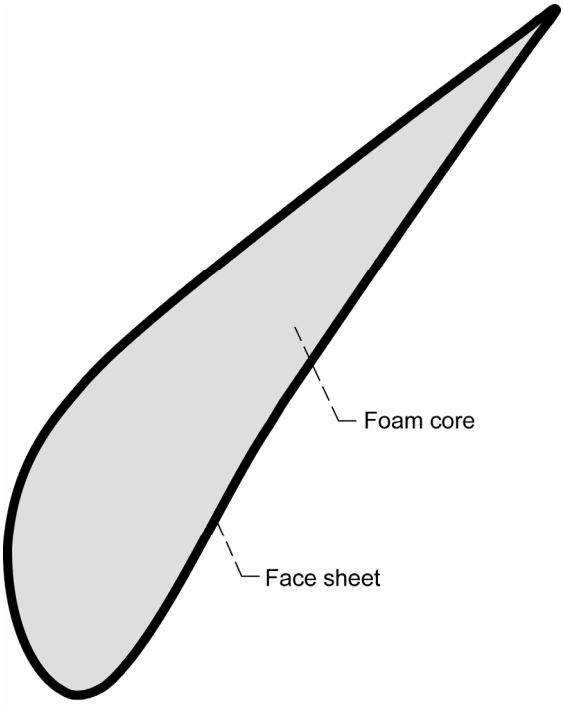

Figure 1.—Schematic of a sandwiched foam fan blade showing the foam core enclosed by the face sheet skin.

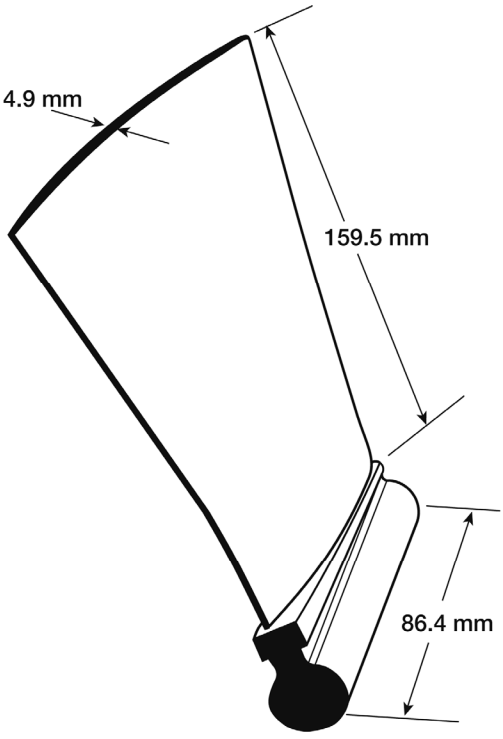

Figure 2.—Schematic of a NASA-designed fan blade with a forward swept profile used in the modeling studies.

[1]National Aeronautics and Space Administration (NASA).
[2]Gibson and Ashby [2] define the "failure" of foams as the point of plastic collapse or extensive creep and not fracture.

2. Loading Conditions on a Fan Blade

A fan blade in an aircraft engine is fixed to a rotating shaft at its root. The actual geometry of a fan blade is fairly complex including a twist and a varying cross-sectional area for aerodynamic reasons, which complicates the development of failure maps. Thus, for simplicity, this paper assumes that the fan blade geometry is a simple cantilevered panel with a uniform rectangular cross-section held rigidly at its root (fig. 3(a)). More detailed analyses would require taking into account the variable geometry of the fan blade. Despite this simplified geometry, it is felt that the failure maps presented here are likely to be representative of the mechanisms governing the failure of these 17-4 PH sandwiched foam fans. As with any deformation [28] and fracture [29] maps, the positions of the regime boundaries on the maps depend both on the accuracy of the equations describing the failure loads as well as the quality of the data used in generating the maps. table 1 lists the mechanical properties data for wrought and heat treated 17-4PH stainless steel obtained from literature sources [30-33].

TABLE 1.—MATERIAL PROPERTY DATA FOR HEAT-TREATED WROUGHT 17-4PH STAINLESS STEEL ALLOY

Property	Units	17-4PH (H-1025 condition)
Density	Mg m^{-3}	7.64 [30]
Poisson's ratio		0.27 [30]
Coefficient of thermal expansion (CTE)	μm m^{-1} K^{-1}	10.8 [31,32]
Shear modulus	GPA	77.2 [33]
Young's modulus	GPa	196.5 [30]
Fatigue Limit	MPa	572 [30]
0.2% Yield strength	MPa	1172 [30]
Ultimate tensile strength	MPa	1276 [30]

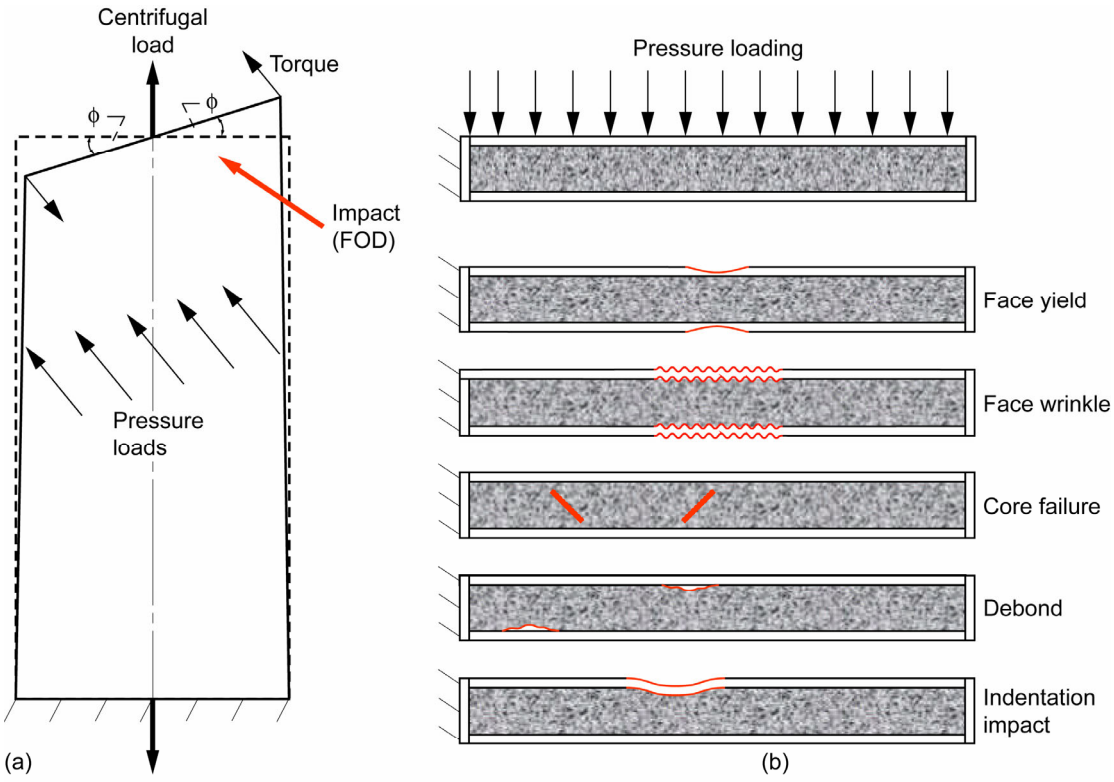

Figure 3.—(a) Schematic showing the different types of loading modes likely to be experienced by of a cantilevered fan blade during service. (b) Schematic of likely modes of failure of a sandwiched foam panel subjected to pressure and impact type loads.

A rotating fan blade experiences several types of loading profiles during service (fig. 3(a)). First, a distributed pressure load, q, acts on the blade due to the action of the air pressure causing bending of the blade leading one surface to be under tensile loading and the opposite surface to be under compressive loading. Under these loading conditions, several failure modes described by Gibson and Ashby [2] (fig. 3(b)), such as face yielding, face wrinkling, foam core failure and debonding at the foam core-face sheet interfaces are equally relevant. Second, torsional loads are generated when the blade twists. In this case, shear stresses develop in the core, face sheets and interfaces, which are likely to fail in shear. Third, the blade also experiences an axial centrifugal loading due to its rotation. This type of loading can lead to tensile yield of the face sheet and foam core and shear failure of the brazed joints. Fourth, the fan blade experiences a localized indentation load, P_{ind}, due to foreign object damage (FOD), where the face sheet and the foam core experience localized plastic yield. The fan blade is constantly subjected to the first three loading conditions during the operation of the aircraft engine and FOD type loading occurs intermittently due to external factors, such as bird strikes and debris swept up from the runway during take-off and landing. Owing to this complex loading profile, failure maps must be generated for each loading mode in order to be meaningful. Since the impact loading on the fan blade due to FOD is a probabilistic event, the maps discussed below do not consider this loading mode.

3. Results and Discussion

3.1 Failure Map for Distributed Pressure Loads

As discussed earlier, four failure modes are likely when a cantilevered sandwiched foam panel representing an idealized fan blade geometry is subjected to air pressure. The failure equations for these modes are identical to those derived by Gibson and Ashby [2] for a specimen subjected to a bend load. The yielding of the face sheets occurs when the normal applied stress exceeds their compressive or tensile yield strength. Thus, the tensile failure load, q, for face yielding is given by [2]

$$q = B_1\, b\, t_c \left(\frac{t}{L}\right) \sigma_{ys} \text{ (face yield)} \tag{1.a}$$

where b is the width of the rectangular sandwiched foam cantilever panel, t is the thickness of the face sheet, t_c is the thickness of the foam core, L is its span length, σ_{ys} is the yield strength of the solid metal and B_1 is a constant equal to 2 for a cantilever panel under a uniformly distributed load [2].

Face sheets under compressive loading can fail by wrinkling as they buckle when the normal stress reaches the local instability stress. Assuming that the foam core has a Poisson's ratio, $\upsilon_c = 0.27$ (table 1), the compressive failure load for face wrinkling is given by [2]

$$q = 0.57 B_1 b\, t_c \left(\frac{t}{L}\right) E_s^{\frac{1}{3}}\, E_{cs}^{\frac{2}{3}} \left(\frac{\rho_c}{\rho_s}\right)^{\frac{4}{3}} \text{ (face wrinkling)} \tag{1.b}$$

where E_s is the Young's modulus of the face sheet, E_{cs} is the Young's modulus of solid unfoamed core, and ρ_c and ρ_s are the densities of the foam core and solid metal, respectively.

The foam core in a cantilevered sandwiched foam panel experiences both normal and shear stresses under a uniformly distributed external load. The failure of the foam core can occur when the principal stresses satisfy the yield criterion. Alternatively, the foam core can undergo shear failure when the shear stress exceeds the shear strength of the foam [2]. The failure load for the foam core failure by shear is given by

$$q = C_1\, b\, t_c \left(\frac{\rho_c}{\rho_s}\right)^{\frac{3}{2}} \sigma_{ys} \quad \text{(Foam core yield)} \tag{1.c}$$

Debonding at the brazed interfaces between the face sheets and the foam core occurs when q exceeds the bond strength of the brazed joints. Thus, the failure load leading to bond failure is given by

$$q = B_2 b\, t_c \left(\frac{t}{L}\right)\left(\frac{G_{\text{critical}}\, E_s}{t}\right)^{\frac{1}{2}} \tag{1.d}$$

where B_2 is a constant equal to 2 for a sandwiched foam cantilever panel [2] and G_{critical} is the critical fracture toughness of the brazed interfaces at which debonding occurs. Despite its simplicity, the application of eq. (1.d) in developing failure maps is complicated by the fact that there appears to be no fracture toughness data available for the BNi-6 brazing alloy used in this study. It is expected that if the face sheets are poorly bonded to the foam core, the sandwich panel will fail by debonding of the brazed joint. Thus, the failure maps presented in this report implicitly assume that the face sheets are well bonded to the foam core and debonding is not the source of failure of the sandwiched panels.

Figure 4 represents the failure map for a sandwiched foam panel subjected to a distributed pressure load plotted as ρ_c/ρ_s versus t/L. In the absence of debonding at the brazed joints, only eqs. (1.a) to (1.c) need be considered for identifying the boundaries of the three failure domains in the $\rho_c/\rho_s - t/L$ space. The locations of the boundaries are obtained by equating the pair of equations describing two adjacent failure mechanisms since the magnitudes of q are identical for both processes at their common boundary. Each failure regime shown on the map then represents the mechanism with the lowest magnitude of q since failure will preferentially occur by this mode when the load reaches this critical value. An examination of figure 4 suggests that the wrinkling of the face sheets is likely to occur when $\rho_c/\rho_s < 0.035$ and $t/L < 0.003$. Thus,

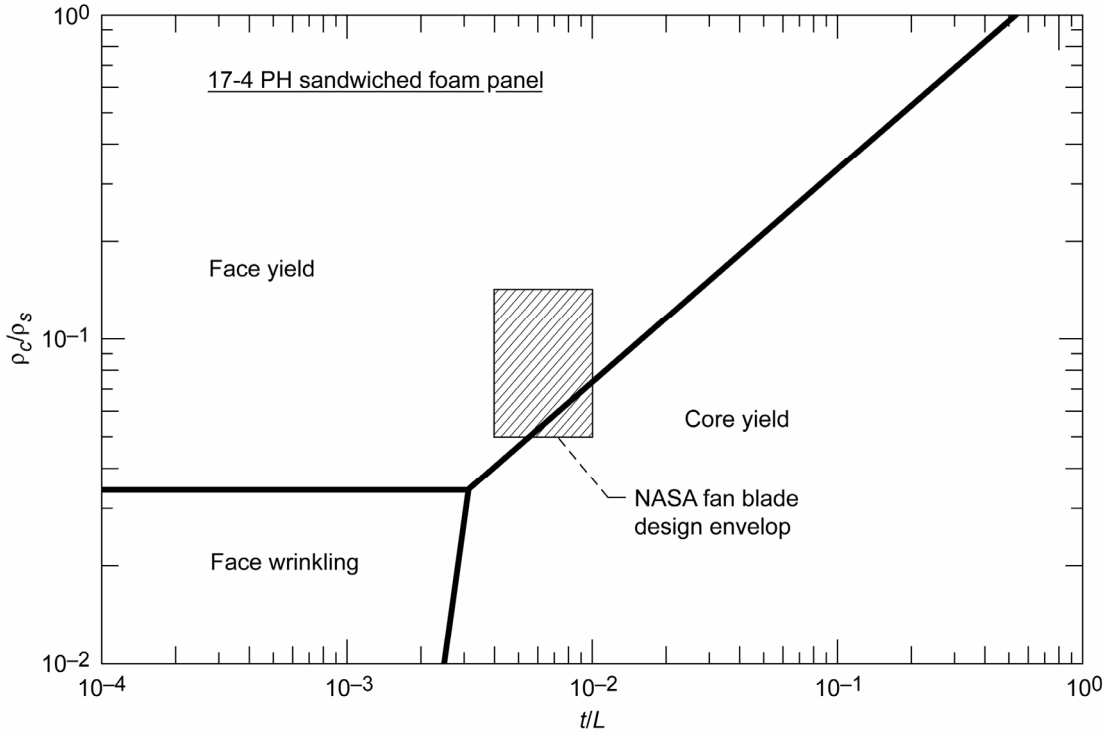

Figure 4.—Failure map for a 17-4 PH sandwiched foam panel subjected to bending under the action of pressure loading.

decreasing the density of the foam core can result in a change in the failure mode from tensile yield of the face sheets to their compressive buckling when the sheets are thin and the span length of the fan blade is relatively long. The transition from the yielding of the face sheet on the tensile surface to the wrinkling of the sheet on the compressive face occurs at a constant value of $\rho_c/\rho_s = 0.035$ independent of the face sheet thickness and the fan blade length.

The failure of the foam core becomes more likely when $t/L > 0.003$. For sandwiched foam panels fulfilling this criterion, failure will occur by either the tensile yielding of the foam core or the yielding of the face sheet at the tensile surface depending on the magnitude of ρ_c/ρ_s. At a constant value of t/L, the probability that the foam core will deform and fail decreases with increasing relative density of the foam core. Correspondingly, at a constant value of t/L, as ρ_c/ρ_s increases the probability that the face sheets will plastically deform will increase Similarly, for a constant value of $\rho_c/\rho_s > 0.035$, the tendency of the foam core to deform and fail increases as the face sheet thickness increases and the fan blade span decreases. The optimum design envelop for the NASA fan blade shown in figure 2 has been evaluated elsewhere [26] and the hatched region in figure 4 represents this envelop. It is clear that the NASA fan blade is likely to fail by either the yielding of the foam core or the face sheet under pressure loading.

3.2. Failure Map under Torsional Loads

The assumption of well-bonded brazed joints resistant to failure leaves only two failure modes to be considered in this analysis. The sandwiched foam panel experiences shear stresses under this type of loading thereby resulting in either the shear failure of the foam core or the face sheets. The maximum shear stresses acting on the face sheets, $(\tau_s)_{max}$, and the foam core, $(\tau_c)_{max}$, are derived in Appendix A. The relationship between the relative density of the sandwiched foam and the normalized thickness, t/t_p, where $t_p = (2t + t_c)$ is the total thickness of the sandwiched foam blade, is reproduced below:

$$\frac{\rho_c}{\rho_s} = \left[\frac{0.4}{(1+\upsilon_s)\left(1-\frac{2t}{t_p}\right)} \right]^2 \tag{2}$$

Figure 5 shows the failure map of the fan blade, plotted as a function of (ρ_c/ρ_s) versus (t/L) to define the location of the boundary between the two failure mechanisms. The solution of the problem leads to non-linear results with the yielding of the foam core being the most likely failure mode for the predicted design range of the sandwiched foam panels. Once again, the hatched region represents the optimized design envelop for the NASA fan blade, where it is evident that it is likely to fail by the failure of the foam core under torsional loading.

3.3. Failure Map for Centrifugal Loading

A rotating sandwiched foam panel also experiences an axial loading force, P, due to its rotation. Since the panel is under a tensile force, face wrinkling is unimportant and only two modes of failure involving the tensile yield of the face sheets and the foam core need be considered. The details of the analysis for axial loading described in Appendix B leads to the transition boundary being located at

$$\left(\frac{\rho_c}{\rho_s}\right) = 0.09 \tag{3}$$

Figure 6 shows the failure map for the 17-4PH sandwiched foam panel under centrifugal axial loading. The transition boundary between the two failure modes is independent of t/L and occurs at a constant value of $\rho_c/\rho_s = 0.09$. For values of $\rho_c/\rho_s < 0.09$, the dominant failure mode is likely to be the yielding of the foam

core. Above this critical value, the failure mode transitions to the yielding of the face sheets. As evident by the hatched region, the optimized NASA fan blade is likely to fail either by the yielding of the foam core or the face sheet under centrifugal axial loading.

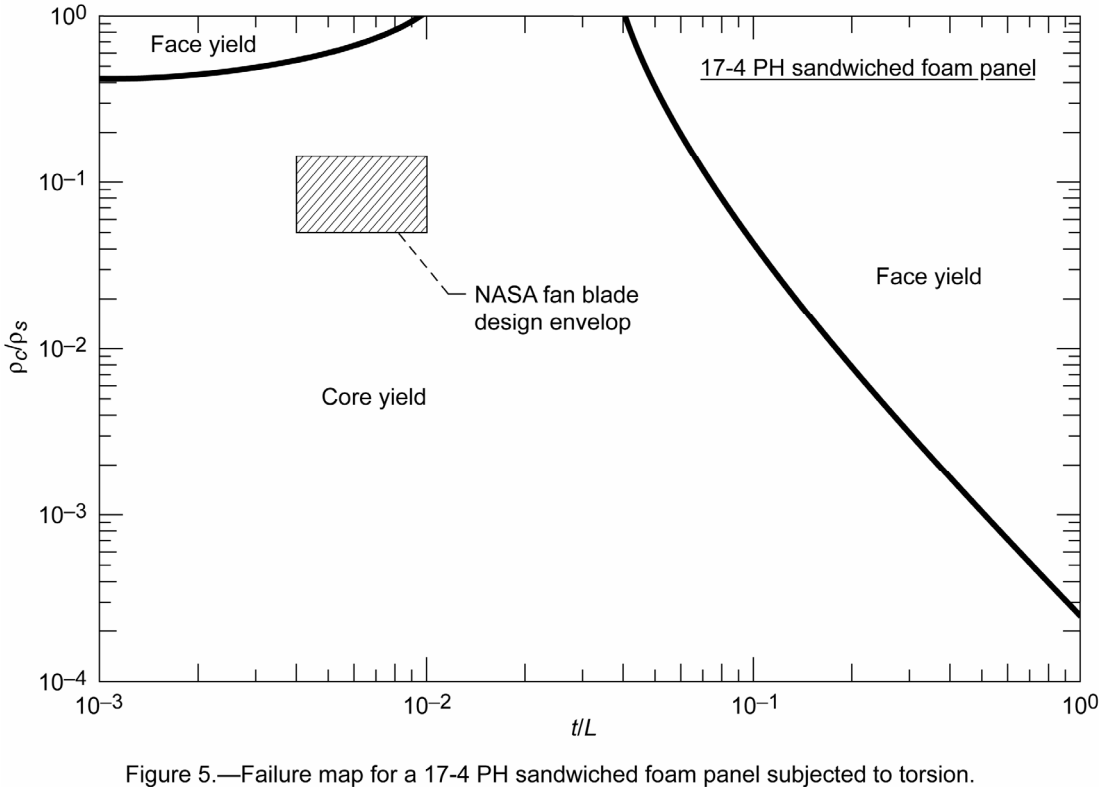

Figure 5.—Failure map for a 17-4 PH sandwiched foam panel subjected to torsion.

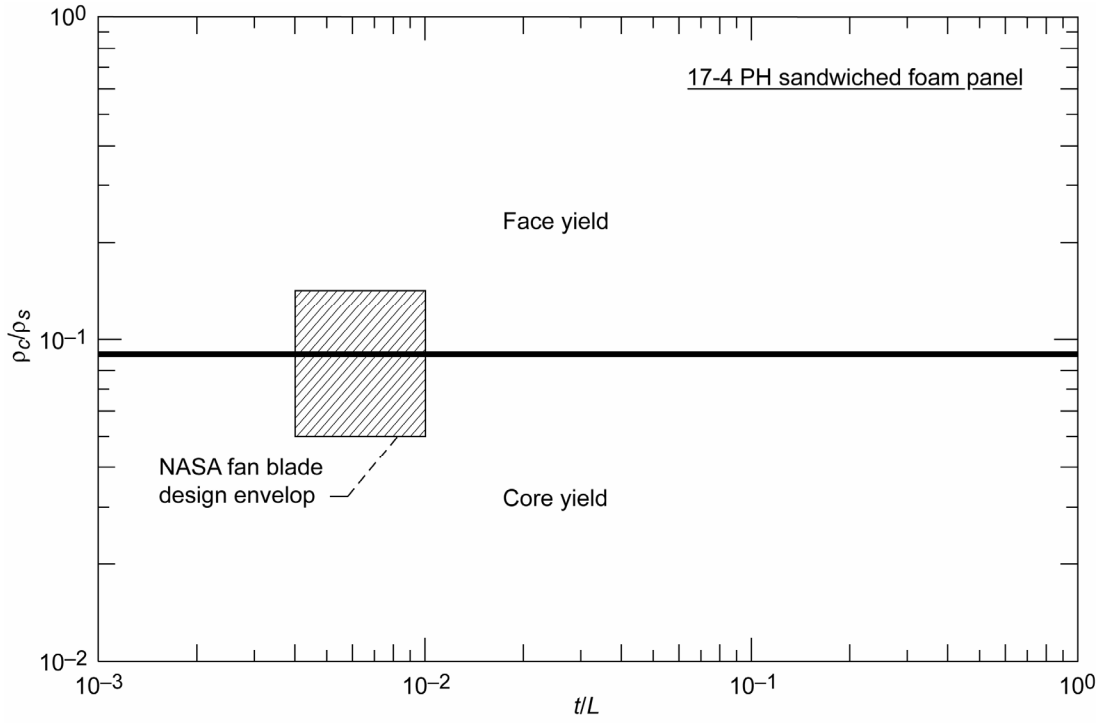

Figure 6.—Failure map for a 17-4 PH sandwiched foam panel subjected to centrifugal axial loading.

4. Summary and Conclusions

Sandwiched foam 17-4PH structures have been proposed for fabricating lightweight and relatively less expensive aircraft engine fan blades [26]. In an attempt to understand probable failure modes in these foam constructed blades under different loading conditions, theoretical failure maps were generated for rectangular 17-4 PH sandwich foam structures assuming that the face sheets were well-bonded to the foam core. Following Gibson and Ashby [2], three foam failure modes were investigated, where the failure maps were constructed as plots of ρ_c/ρ_s versus t/L. Three types of loading conditions were considered in an attempt to simulate three different types of loads experienced by an idealized aircraft engine fan blade: centrifugal load, pressure distributed bend load, and torsional load. The failure maps for the 17-4PH sandwiched foam structures suggest that face wrinkling, face yield and foam core yield are the main modes of failure under a pressure distributed bend load depending on the magnitudes of ρ_c/ρ_s and t/L. However, face and foam core yielding are the two probable modes of failure under torsional and centrifugal tensile loads.

The design envelop for a NASA-designed fan blade was superimposed on the maps. As a result, the insights provided by the maps suggest that the yielding of the faces and the foam core are the two important failure modes for the NASA fan blade under centrifugal axial loading and pressure distributed bend load conditions. However, the fan blade is likely to fail solely by the yielding of the foam core under torsional loads.

Appendix A—Derivation of Maximum Shear Stresses Acting on a Sandwiched Foam Panel Under Torsional Loading

For simplicity, the sandwiched foam fan blade is assumed to be a cantilever panel of length, L, width, b, and thickness, t_p (= $2t + t_c$), subject to a total torsional load, T, in this analysis (fig. A.1). When the face sheets are fully bonded to the foam core, the total strain, ε_T, equals the strain in the foam core, ε_c, and that in the face sheets, ε_s, (i.e. $\varepsilon_T = \varepsilon_c = \varepsilon_s$). From static equilibrium, the total torque is equal to the sum of the torques, T_c and T_s acting on the core and the face sheets, respectively, given by

$$T = T_c + T_s \tag{A.1}$$

Since the twist angle, ϕ, is identical for both the foam core and the face sheets,

$$\phi = \frac{T_c L}{G_c I_{pc}} = \frac{T_s L}{G_s I_{ps}} \tag{A.2}$$

where L is the span of the fan blade, G_c and G_s are the shear moduli of the foam core and the face sheets, respectively, and I_{pc} and I_{ps} are the polar moments of inertia for the foam core and face sheets, respectively, given by

$$I_{pc} = \left[\frac{(b-2t)(t_p-2t)\left\{(b-2t)^2 + (t_p-2t)^2\right\}}{12}\right] \quad \text{(foam core)} \tag{A.3.a}$$

$$I_{ps} = \left[\frac{2t(b-t)^2(t_p-t)^2}{\left\{(b-t)+(t_p-t)\right\}}\right] \quad \text{(face sheet)} \tag{A.3.b}$$

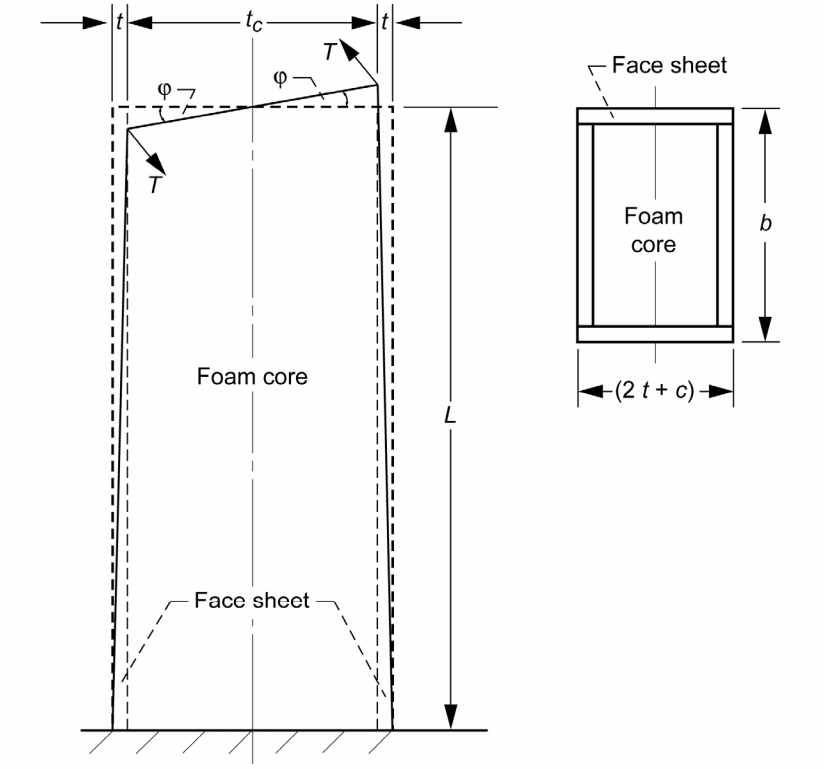

Figure A.1.—Schematic of a cantilevered sandwiched foam panel under torsion.

The magnitude of G_c can be determined from eq. (A.4.a) [2]

$$G_c = \frac{3}{8} E_s \left(\frac{\rho_c}{\rho_s} \right)^2 \tag{A.4.a}$$

while that of G_s is given by

$$G_s = \left[\frac{E_s}{2(1+\upsilon_s)} \right] \tag{A.4.b}$$

where υ_s is the Poisson's ratio is the solid material. Solving eq. (A.1) and (A.2) gives

$$T_c = T \left(\frac{G_c I_{pc}}{(G_c I_{pc} + G_s I_{ps})} \right) \text{ (foam core)} \tag{A.5.a}$$

$$T_s = T \left(\frac{G_s I_{ps}}{(G_c I_{pc} + G_s I_{ps})} \right) \text{ (foam core)} \tag{A.5.b).}$$

The maximum shear stresses, $(\tau_c)_{max}$ and $(\tau_s)_{max}$, acting on the foam core and face sheets, respectively, are then given by

$$(\tau_c)_{\max} = G_c \gamma = \frac{G_c r \phi}{L} = \frac{T_c r}{I_{pc}} = \left(\frac{T_c}{I_{pc}} \right) \left(\frac{t_p}{2} - t \right) \text{ (foam core)} \tag{A.6.a}$$

$$(\tau_s)_{\max} = G_s \gamma = \frac{G_s r \phi}{L} = \frac{T_s r}{I_{ps}} = \left(\frac{T_s}{I_{ps}} \right) \left(\frac{t_p}{2} \right) \text{ (face sheet)} \tag{A.6.b}$$

where γ is the shear strain and r is the radial distance across the fan blade cross-section. Substituting eqs. (A.5.a) and (A.5.b) into eqs. (A.6.a) and (A.6.b),

$$(\tau_c)_{\max} = T \left[\frac{G_c}{\{G_c I_{pc} + G_s I_{ps}\}} \right] \left(\frac{t_p}{2} - t \right) \tag{A.7.a}$$

$$(\tau_s)_{\max} = T \left[\frac{G_s}{\{G_c I_{pc} + G_s I_{ps}\}} \right] \left(\frac{t_p}{2} \right) \tag{A.7.b}$$

Thus,

$$\frac{(\tau_c)_{\max}}{(\tau_s)_{\max}} = \frac{G_c}{G_s} \left(1 - \frac{2t}{t_p} \right) \tag{A.8}$$

Using eqs. (A.4.a) and (A.4.b), eq. (A.8) reduces to

$$\frac{(\tau_c)_{\max}}{(\tau_s)_{\max}} = \frac{3}{4}(1+\upsilon_s)\left(\frac{\rho_c}{\rho_s}\right)^2\left(1-\frac{2t}{t_p}\right) \tag{A.9}$$

Failure of the foam core is assumed to occur when yielding first takes place i.e. when $(\tau_c)_{\max} = 0.5\sigma_{yc}$. Thus, using eq. (A.10) [2],

$$\frac{\sigma_{yc}}{\sigma_{ys}} \approx 0.3\left(\frac{\rho_c}{\rho_s}\right)^{3/2} \tag{A.10}$$

$$(\tau_c)_{\max} = 0.15\left(\frac{\rho_c}{\rho_s}\right)^{\frac{3}{2}}\sigma_{ys} \tag{A.11}$$

Similarly, assuming that the face sheet failure criterion is $(\tau_s)_{\max} = 0.5\sigma_{ys}$ and substituting for $(\tau_c)_{\max}$ using eq. (A.11) and $(\tau_s)_{\max}$ in eq. (A.9), the relationship between the relative density of the sandwiched foam and the normalized thickness, t/t_p is given by

$$\frac{\rho_c}{\rho_s} = \left[\frac{0.4}{(1+\upsilon_s)\left(1-\frac{2t}{t_p}\right)}\right]^2 \tag{A.12}$$

Appendix B—Derivation of Maximum Stresses Acting on the Sandwiched Foam Panel Under Axial Loading Conditions

A fan blade will experience an axial loading force, P, during its rotation. This load is carried in part by the face sheets and in part by the foam core represented by forces P_s and P_c, respectively. For a sandwiched foam panel of mass, m_T, undergoing an acceleration, a_T, the differential axial force acting on it due to rotation is

$$\delta P = \delta m_T a_T = P_s + P_c \tag{B.1}$$

Noting that $a_T = \omega^2 r$ and $m_T = \rho_c A_c r + \rho_s A_s r$, where A_c and A_s are the cross-sectional areas of the foam core and the face sheets, respectively, eq. (B.1) can be expressed as

$$\delta P = (\rho_c A_c + \rho_s A_s)\, \omega^2 r\, \delta r = \delta P_s + \delta P_c \tag{B.2}$$

When the face sheets are fully bonded to the foam core, the total strain, ε_T, equals the strain in the foam core, ε_c, and that in the face sheets, ε_s, (i.e. $\varepsilon_T = \varepsilon_c = \varepsilon_s$). Failure of the sandwiched foam panel is assumed to occur when it first begins to yield so that

$$\delta\varepsilon_c = \frac{\delta\sigma_c}{E_c} = \frac{\delta P_c}{A_c E_c} \tag{B.3.a}$$

$$\delta\varepsilon_s = \frac{\delta\sigma_s}{E_s} = \frac{\delta P_s}{A_s E_s} \tag{B.3.b}$$

where σ_c and σ_s are the axial stresses in the foam core and face sheets, respectively, E_c is the elastic modulus of the foam core given by eq. (1), A_c and A_s are the cross-sectional areas of the foam core and the face sheets, respectively. Equating eqs. (B.3.a) and (B.3.b) in order to satisfy compatibility conditions, we have

$$\delta P_s = \delta P_s \left(\frac{A_s E_s}{A_c E_c} \right) \tag{B.4}$$

Substituting eq. (B.6) into eq. (B.2) and simplifying the results, the differential forces acting on the foam core and the face sheets can be expressed as

$$\delta P_c = \left[\frac{A_c E_c (\rho_s A_s + \rho_c A_c)\omega^2}{(A_s E_s + A_c E_c)} \right] r\delta r \tag{B.5.a}$$

$$\delta P_s = \left[\frac{A_s E_s (\rho_s A_s + \rho_c A_c)\omega^2}{(A_s E_s + A_c E_c)} \right] r\delta r \tag{B.5.b}$$

Thus,

$$\delta\sigma_c = \frac{\delta P_c}{A_c} = \left[\frac{E_c (\rho_s A_s + \rho_c A_c)\omega^2}{(A_s E_s + A_c E_c)} \right] r\delta r \tag{B.6}$$

The elastic modulus of the foam core is given by [2]

$$E_c = E_s\left(\frac{\rho_c}{\rho_s}\right)^2 \tag{B.7}$$

Combining eqs. (B.6) and (B.7), we have

$$\delta\sigma_c = \left[\left\{\left(\frac{\rho_c}{\rho_c}\right)^2 E_s\right\}\frac{(\rho_s A_s + \rho_c A_c)\omega^2}{(A_s E_s + A_c E_c)}\right] r\delta r \tag{B.8.a}$$

and

$$\delta\sigma_s = \frac{\delta P_s}{A_s} = \left[\frac{E_s(\rho_s A_s + \rho_c A_c)\omega^2}{(A_s E_s + A_c E_c)}\right] r\delta r \tag{B.8.b}$$

The yield strength of an ideal foam core without any manufacturing defects is given by [2]

$$\left(\frac{\sigma_{yc}}{\sigma_{ys}}\right) = 0.3\left(\frac{\rho_c}{\rho_s}\right)^{3/2} \tag{B.9}$$

At the proportional limit, $\sigma_c = \sigma_{yc}$ and $\sigma_s = \sigma_{ys}$, so that from eqs. (B.8.a), (B.8.b) and (B.9) the boundary between the yield of the face sheet and the foam core is given by

$$\left(\frac{\rho_c}{\rho_s}\right)^2 = 0.3\left(\frac{\rho_c}{\rho_s}\right)^{3/2} \tag{B.10}$$

Simplifying,

$$\left(\frac{\rho_c}{\rho_s}\right) = 0.09 \tag{B.11}$$

References

1. J.S. Huang, Y. Lin, Acta Mater., **44** (1996) 289-296.
2. L.J. Gibson, M.F. Ashby, *Cellular Solids: Structure and Properties*, Cambridge University Press, Cambridge, U.K. (1997).
3. J.L. Grenestedt, J. Mech. Phys. Solids, **46** (1998) 29-50.
4. A. Evans, J.W. Hutchinson, M.F. Ashby, Prog. Mater. Sci., **43** (199) 171–221.
5. A.M. Harte, N.A. Fleck, M.F. Ashby, Advan. Enging. Mater., **2** (2000) 219-222.
6. M.F. Ashby, A.G. Evans, N.A. Fleck, L.J. Gibson, J.W. Hutchinson, H.N.G. Wadley, *Metal Foams: A Design Guide*, Butterworth-Heinemann, Boston, MA (2000).
7. J.C. Wallach, L.J. Gibson, Intern. J. Solids and Struct., **38** (2001) 7181-7196.
8. A.E. Markaki, T.W. Clyne, Acta Mater. **49** (2001) 1677-1686.
9. A.E. Markaki, T.W. Clyne, Acta Mater. **51** (2003) 1341-1350.
10. A.E. Markaki, T.W. Clyne, Acta Mater. **51** (2003) 1351-1357.
11. E.E. Gdoutos, I.M. Daniel, K.A. Wang, Mech. Mater., **35** (2003) 511-522.
12. O. Kesler, L. K. Crews, L.J. Gibson, Mater. Sci. Eng., **A341** (2003) 264-272.
13. H. Harders, K. Hupfer, J. Rösler, Acta Mater., **53** (2005) 1335-1345.
14. J.L. Grenestedt, J. Mater. Sci., **40** (2005) 5853-5857.
15. M.H. Luxner, J. Stampfl, H.E. Petermann, J. Mater. Sci., **40** (2005) 5859-5866.
16. H.S. Zurob, Y. Bréchet, J. Mater. Sci., **40** (2005) 5893-5901.
17. S. Forest, J.S. Blazy, Y. Chastel, F. Moussy, J. Mater. Sci., **40** (2005) 5903-5910.
18. C. Tekoglu, P.R. Onck, J. Mater. Sci., **40** (2005) 5911-5917.
19. J.A. Rongong, R.J. Williams, "Lightweight, Polymeric Cavity Filler for Damping Hollow Fan Blade Vibrations," http://www.hcf.utcdayton.com/papers/0330 Rongong.pdf, Proc. 9th National Turbine Engine High Cycle Fatigue (HCF) Conference, Pinehurst, NC, March 16-19, 2004.
20. Y. Conde, A. Pollien, A. Mortensen, Scripta Mater. **54** (2006) 539-543.
21. J. Banhart, Prog. Mater. Sci., **46** (2001) 559–632.
22. A.A. Shirzadi, M. Kocak, E.R. Wallach, Sci. Techn. Weld. Join., **9** (2004) 277-279.
23. A. Salimon, Y. Bréchet, M. F. Ashby, A. L. Greer, J. Mater. Sci., **40** (2005) 5793-5799.
24. S.J. Mullen, "I-Beam Honeycomb Material," U.S. Patent No. 4,632,862 (1986).
25. J.F. Newton, T.D. Martin, N. Willard, D.J. Carbery, R. Ikegami, "Lightweight Honeycomb Panel Structure," U.S. Patent No. 5,445,861 (1995).
26. S.V. Raj, L.J. Ghosn, B.A. Lerch, M. Hebsur, L.M. Cosgriff, M. Topolski, "An Evaluation of Lightweight Stainless Steel Foam Design Concepts for Fan and Propeller Blade Applications," NASA/TM—2005-213620, Glenn Research Center, Cleveland, OH (2005).
27. S.V. Raj, L.J. Ghosn, B.A. Lerch, M. Hebsur, L.M. Cosgriff and J. Fedor, Mater. Sci. Eng. **456** (2007) 305–316.
28. H.J. Frost, M.F. Ashby, *Deformation Mechanism Maps: The Plasticity and Creep of Metals and Ceramics*, Pergamon, Oxford (1982).
29. C. Gandhi, M.F. Ashby, Acta Metall. **27** (1979) 1565-1602.
30. *Structural Alloy Handbook*, J.M. Holt, C.Y. Ho (eds.), CINDAS, Purdue University, West Lafayette, IN (1996).
31. Advanced Materials & Processes: Guide to Engineered Materials, **159** (2002) ASM International, Materials Park, OH.
32. "17-4PH Stainless Steel Product Data Sheet." http://www.aksteel.com/pdf/markets_products/Stainless/precipitation/17-4_PH_Data_Sheet.pdf, AK Steel Corp., Middletown, OH (2004).
33. *Metallic Materials Properties Development and Standardization (MMPDS)*, Chapter 2.6.9, U. S. Department of Transportation, Knovel Library, http://www.knovel.com/knovel2/.jsp?BookID=1083&VerticalID=0, pp. 2-195 to 2-212, (2003).

REPORT DOCUMENTATION PAGE	Form Approved OMB No. 0704-0188

1. REPORT DATE *(DD-MM-YYYY)*	2. REPORT TYPE	3. DATES COVERED *(From - To)*
31-05-2007	Technical Memorandum	

4. TITLE AND SUBTITLE
Failure Maps for Rectangular 17-4PH Stainless Steel Sandwiched Foam Panels

5a. CONTRACT NUMBER

5b. GRANT NUMBER

5c. PROGRAM ELEMENT NUMBER

6. AUTHOR(S)
Raj, S., V.; Ghosn, L., J.

5d. PROJECT NUMBER

5e. TASK NUMBER

5f. WORK UNIT NUMBER
WBS 561581.02.08.03.04.03

7. PERFORMING ORGANIZATION NAME(S) AND ADDRESS(ES)
National Aeronautics and Space Administration
John H. Glenn Research Center at Lewis Field
Cleveland, Ohio 44135-3191

8. PERFORMING ORGANIZATION REPORT NUMBER
E-15935

9. SPONSORING/MONITORING AGENCY NAME(S) AND ADDRESS(ES)
National Aeronautics and Space Administration
Washington, DC 20546-0001

10. SPONSORING/MONITORS ACRONYM(S)
NASA

11. SPONSORING/MONITORING REPORT NUMBER
NASA/TM-2007-214802

12. DISTRIBUTION/AVAILABILITY STATEMENT
Unclassified-Unlimited
Subject Categories: 07, 26, 05, and 01
Available electronically at http://gltrs.grc.nasa.gov
This publication is available from the NASA Center for AeroSpace Information, 301-621-0390

13. SUPPLEMENTARY NOTES
Published in Materials Science and Engineering: A.

14. ABSTRACT
A new and innovative concept is proposed for designing lightweight fan blades for aircraft engines using commercially available 17-4PH precipitation hardened stainless steel. Rotating fan blades in aircraft engines experience a complex loading state consisting of combinations of centrifugal, distributed pressure and torsional loads. Theoretical failure plastic collapse maps, showing plots of the foam relative density versus face sheet thickness, t, normalized by the fan blade span length, L, have been generated for rectangular 17-4PH sandwiched foam panels under these three loading modes assuming three failure plastic collapse modes. These maps show that the 17-4PH sandwiched foam panels can fail by either the yielding of the face sheets, yielding of the foam core or wrinkling of the face sheets depending on foam relative density, the magnitude of t/L and the loading mode. The design envelop of a generic fan blade is superimposed on the maps to provide valuable insights on the probable failure modes in a sandwiched foam fan blade.

15. SUBJECT TERMS
17-4PH; Stainless steel; Metallic foams; Sandwiched foam panel; Theoretical failure maps; Design

16. SECURITY CLASSIFICATION OF:			17. LIMITATION OF ABSTRACT	18. NUMBER OF PAGES	19a. NAME OF RESPONSIBLE PERSON
a. REPORT	b. ABSTRACT	c. THIS PAGE			S.V. Raj
U	U	U		21	19b. TELEPHONE NUMBER *(include area code)* 216-433-8195